NIST Technical Note
NIST TN 2321

Polycyclic Aromatic Hydrocarbons Analysis in Propene Smoke Using Thermal Desorption-Gas Chromatography-Mass Spectrometry

Aika Davis
Ryan Falkenstein-Smith
Thomas Cleary

This publication is available free of charge from:
https://doi.org/10.6028/NIST.TN.2321

NIST NATIONAL INSTITUTE OF STANDARDS AND TECHNOLOGY
U.S. DEPARTMENT OF COMMERCE

NIST Technical Note
NIST TN 2321

Polycyclic Aromatic Hydrocarbons Analysis in Propene Smoke Using Thermal Desorption-Gas Chromatography-Mass Spectrometry

Aika Davis
Ryan Falkenstein-Smith
Thomas Cleary
Fire Research Division
Engineering Laboratory

This publication is available free of charge from:
https://doi.org/10.6028/NIST.TN.2321

December 2024

U.S. Department of Commerce
Gina M. Raimondo, Secretary

National Institute of Standards and Technology
Laurie E. Locascio, NIST Director and Under Secretary of Commerce for Standards and Technology

Certain equipment, instruments, software, or materials, commercial or non-commercial, are identified in this paper in order to specify the experimental procedure adequately. Such identification does not imply recommendation or endorsement of any product or service by NIST, nor does it imply that the materials or equipment identified are necessarily the best available for the purpose.

Publication History
Approved by the NIST Editorial Review Board on 2024-12-06

How to cite this NIST Technical Series Publication:
Davis AY, Falkenstein-Smith RL, Cleary TG (2024) Polycyclic Aromatic Hydrocarbons Analysis in Propene Smoke Using Thermal Desorption-Gas Chromatography-Mass Spectrometry. (National Institute of Standards and Technology, Gaithersburg, MD), NIST TN 2321. https://doi.org/10.6028/NIST.TN.2321

Author ORCID iDs
Aika Davis: 0000-0001-8620-5311
Ryan Falkenstein-Smith: 0000-0001-7039-5835
Thomas Cleary: 0000-0001-8785-2035

Contact Information
aika.davis@nist.gov

Abstract

A new method to analyze polycyclic aromatic hydrocarbons (PAHs) in both gas and particulate samples using one instrument setup is presented. PAHs make up soot in smoke; PAHs in non-sooting to soot-dominant smoke in the overfire region were collected and analyzed by using thermal desorption - gas chromatography-mass spectrometry (TD-GC/MS). Thirty-one PAHs were identified from propene fire smoke, primarily in soot. This method is efficient and versatile; it will be used to gather more PAH yields from various fuel sources and to monitor ambient PAH concentrations.

Keywords

polycyclic aromatic hydrocarbon; gas chromatography; propene smoke; soot.

Table of Contents

List of Tables

List of Figures

Author Contributions

Aika Davis: Methodology, Data curation, Writing- Original draft preparation, Software.

Ryan Falkenstein-Smith: Conceptualization, Methodology, Writing- Reviewing and Editing.

Thomas Cleary: Conceptualization, Methodology, Data curation, Supervision.

1. Introduction

Polycyclic aromatic hydrocarbons (PAHs), hydrocarbons containing two or more aromatic rings, may present serious health risks (e.g., cancer, immunotoxicity, neurodegenerative disorders, and organ damage to kidneys, liver, and reproductive system) to those exposed to them [1, 2]. The International Agency for Research on Cancer lists benz[a]anthracene and benzo[a]pyrene as likely carcinogenic to humans and benzo[b]fluoranthene, benzo[j]fluoranthene, benzo[k]fluoranthene, and indeno[1,2,3-c,d]pyrene as possibly carcinogenic to humans [3]. Certain PAHs, such as acenaphthene, acenaphtylene, anthracene, benzo(g,h,i)perylene, fluorene, phenanthrene, and pyrene, have been listed on the U.S. Environmental Protection Agency's (EPA's) Priority Chemical List, which is informative to risk management regulations during exposure events [4]. At a fire scene, PAHs can be released into the atmosphere from incomplete combustion of organic materials (e.g., crude oil, wood, and other hydrocarbon fuels), creating the risk of inhalation, oral injestion, and/or dermal exposure.

In the context of fire science, a study found that PAH levels increased during a wildfire event, three times higher than the monthly average for the site studied [5]. A explanation for the higher concentration could be attributed to the initial formation of soot using PAHs. PAHs are the main precursors to soot formation during incomplete combustion. The general process for the formation of PAHs and their growth to soot, as detailed in [6], are as follows:

1. Formation of heavy PAH molecules
2. Inception of non-organic carbon particles from heavy PAH molecules
3. Growth of particles from the absorption of gas-phase, stable, and radical PAHs
4. Coagulation via particle-particle collisions

Several works [7–21] have focused on establishing formation pathways of soot from PAHs, speculating about the mechanisms of soot inception from heavy PAH molecules in the gas-phase. A major challenge in understanding soot's inception is identifying the transition point between gas-phase PAHs and nano-organic carbon (i.e., "infant soot"). Recent studies [22–26] have implemented experimental and computational techniques to identify this transition point.

In this work, a novel sampling and analytical technique that extracts and then quantifies PAHs retained on particulates as well as those in the gas phase is presented. The technique leverages a thermal-desorption methodology combined with a gas-chromatography/mass-spectrometry system (TD-GC/MS) to analyze PAHs sampled in the vapor phase and on particles, both of which are extracted from smoke plumes. The novelty of the presented technique is in its analysis of PAHs on soot particulates. Previous techniques [5, 27–30] focused on measuring chemical components on particulates, typically obtained from solvent extraction of particulates and soot, are limited in application. Due to its carbonaceous composition, soot is highly retentive towards surrounding heavy chemicals in the gas

phase, which requires a significant portion of solvent to extract retained substances. The large volume of solvent required dilutes the extracted components in the analyzed sample, which may then fall under the limits of detection. The extraction of a larger soot sample is a potential way to address the dilution issue but is not always achievable in application for small fire scenarios. Additionally, extraction on particulates only covers particulate-phase PAHs and neglects to quantify volatile PAHs. In the presented approach here, the thermal-desorption methodology is applied to soot particles, such that analytes of interest are desorbed from an extracted smoke sample and directly introduced to a GC/MS for analysis, thus eliminating the solvent extract process. The thermal-desorption methodology is also applied to a gas phase sample (on sorption media) collected simultaneously as the soot sample.

The purpose of this work is to demonstrate the novel approach for measuring PAHs in particulate matter as well as in the gas phase. The technique is applied to examine the differences in PAH yields of non-sooting to soot-dominant smoke in the overfire region above the laminar flame smoke point, generated by a Santoro burner [31]. The generator utilizes a co-flow burner that modifies fuel/air intake to generate varying concentrations of soot. The application of this technique in the aerosol generator design showcases its benefits as well as highlights its novelty compared to other analysis approaches.

2. Description of Experiments

2.1. Soot generator

All soot samples collected in this work for analysis were sampled from a laminar propene diffusion flame maintained in a co-flow Santoro burner [31, 32], referred to in this work as a "soot generator." An image of the generator is shown in Fig. 1. The burner included a 12.00 cm diameter ceramic honeycomb used for airflow surrounding a 1.00 cm diameter fuel line in its center. A 53.00 cm long brass burner chimney was positioned on top of the burner. The chimney was equipped with a tripper plate used to induce mixing and an air injection port to dilute the exhaust stream. For this work, propene flow ranged from 0.000 SLPM to 0.050 SLPM (five flow conditions), while the co-flow of air in the burner and dilution air in the chimney were maintained at constant flows of 50.00 SLPM and 30.00 SLPM, respectively. Fuel and air flows fed into the burner were controlled via mass flow controllers with an uncertainty of 1.0 % of the full-scale range, as reported by the manufacturer.

The variance in propene flow allowed the flame to be maintained below and above its sooting point (0 LPM to 0.05 LPM of propene), thus altering the generated soot concentration. For each experiment, soot concentrations were monitored by a tapered element oscillating microbalance (TEOM) which has a combined relative uncertainty of 1 $\mu g/m^3$. The soot concentration was observed, via the TEOM, to range between 0 mg/m^3 and 85 mg/m^3 with a propene flow of 0.000 LPM to 0.050 LPM, respectively.

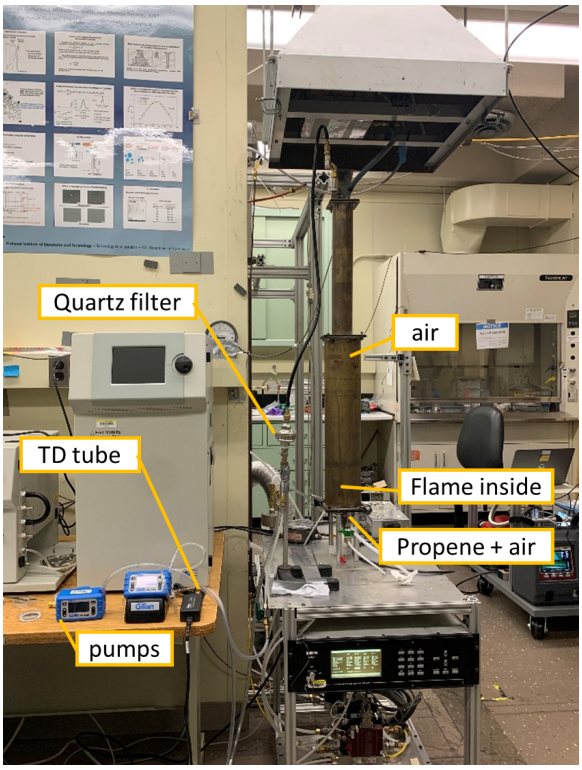

Fig. 1. Experimental setup.

2.2. Sample collection

Soot produced from the generator was extracted from the chimney's sampling port using a portable gas sampling pump and a rough pump to introduce samples onto a thermal desorption (TD) tube and a quartz filter, respectively. The TD tube used (C2-AAXX-5138, Markes International, Llantrisant, UK) was designed to retain PAH substances in the gas phase via a selective retentive material (which is proprietary). For each experiment, gas samples were extracted into the TD tube at flow rates of 0.250 LPM for a 20 min sampling period.

Soot particulates were collected onto a 47 mm diameter quartz filter to estimate the soot yield of the burner. The mass of soot was determined using a well-established gravimetric technique [33, 34]. Before each experiment, a desiccated quartz filter was weighed. During an experiment, the filter was contained in a stainless steel holder (PALL 2220) positioned within a gas sampling line that extracted samples at a flow rate of 2.500 LPM, simultaneously with the portable gas sampling pump used for TD tube sample collection.

2.3. PAH concentration measurements

In this work, an analytical method was constructed to measure the concentration of 31 PAHs, listed in Table 1. The PAH analytes of interest were selected based on the developed standard reference material for aromatic hydrocarbons, SRM2260a. Concentration measurements were made using an Agilent 8890 gas chromatograph equipped with a 5977B series mass spectrometer (GC/MS). The samples were introduced into the GC/MS using an automated thermal desorption system (TD100-xr, Markes International, Llantrisant, UK) that connected to the GC inlet.

Table 1. PAH target analytes (Target) and internal standards (ISTD) and their respective molecular weights (MW), elution times, and quantifier (Quant) and qualifier (Qual) ions used in quantification analysis.

Analyte	MW (amu)	Elution Time (min)	Quant Ion (m/z)	Qual Ion (m/z)	Type
Naphthalene_d8	136	10.2	136	136	ISTD
Naphthalene*	128	10.3	128	129	Target
Biphenyl_d10	164	14.7	164	164	ISTD
Biphenyl	154	14.8	154	153	Target
Acenaphthylene*	152	17.2	152	153	Target
Acenaphthene_d10	164	17.7	164	164	ISTD
Acenaphthene*	154	17.9	153	154	Target
Fluorene*	166	20.3	166	165	Target
Dibenzothiophene	184	24.8	184	139	Target
Phenanthrene_d10	188	25.3	188	188	ISTD
Phenanthrene*	178	25.4	178	179	Target
Anthracene*	178	25.7	178	179	Target
4H-Cyclopenta[def]phenanthrene	190	28.6	190	189	Target
Fluoranthene_d10	212	31.8	212	212	ISTD
Fluoranthene*	202	32.0	202	101	Target
Pyrene_d10	212	33.3	212	212	ISTD
Pyrene*	202	33.4	202	101	Target
Benzo[ghi]fluoranthene	226	39.2	226	224	Target
Benzo[c]phenanthrene	228	39.2	228	227	Target
Benz[a]anthracene_d12	240	40.3	240	240	ISTD
Benz[a]anthracene**	228	40.5	228	229	Target
Cyclopenta[cd]pyrene	226	40.9	226	227	Target
Chrysene**	228	40.9	228	226	Target
Triphenylene	228	41.0	228	226	Target
Benzo[b]fluoranthene**	252	49.0	252	253	Target
Benzo[k]fluoranthene**	252	49.1	252	253	Target

Table 1 Continued: PAH target analytes (Target) and internal standards (ISTD) and their respective molecular weights (MW), elution times, and quantifier (Quant) and qualifier (Qual) ions used in quantification analysis.

Benzo[j]fluoranthene	252	49.2	252	253	Target
Benzo[a]fluoranthene	252	49.8	252	250	Target
Benzo[e]pyrene	252	51.3	252	250	Target
Benzo[a]pyrene_d12	264	51.4	264	264	ISTD
Benzo[a]pyrene**	252	51.6	252	253	Target
Perylene_d12	264	52.2	264	264	ISTD
Perylene	252	52.4	252	253	Target
Dibenz[a,j]anthracene	278	57.6	278	279	Target
Dibenz[a,h]anthracene_d14	292	58.4	292	292	ISTD
Dibenz[a,c]anthracene	278	58.5	278	279	Target
Indeno[1,2,3-cd]pyrene**	276	58.6	276	138	Target
Dibenz[a,h]anthracene**	278	58.6	278	279	Target
Benzo[b]chrysene	278	59.6	278	279	Target
Picene	278	60.1	278	279	Target
Benzo[ghi]perylene_d12	288	60.7	288	288	ISTD
Benzo[ghi]perylene*	276	60.9	276	138	Target

* On EPA's 16-PAH list

** On EPA's 16 and 7-PAH list

As stated in Section 2.2, the TD tubes used in this study (C2-AAXX-5138) were designed to retain PAH analytes in the gas phase. The thermal desorption technique implemented in this study utilized a focus trap (U-T19PAH-2S, Markes International, Llantrisant, UK) also designed to retain PAHs. The desorption conditions used for the TD tube and soot filter analysis are presented in Table 2. For PAH analysis on soot particulates, the desorption process operated at a higher desorption temperature (350 °C) and a longer desorption time (>10 min).

A single GC/MS method for PAH analysis, reported in Table 3, was used for TD tube and soot filter analysis. A Restek Rxi-PAH 60 m x 0.25 mm x 0.1 µm gas chromatography column was chosen to adequately separate PAH analytes. The total run time for the GC/MS analysis method was approximately 100 min when operated at a constant flow of 1.7 mL/min.

As shown in Table 1, two ions were selected for each analyte, determined from the highest (i.e., most abundant) and second-highest (i.e., second most abundant) mass-to-charge ratio (m/z) signal. The most abundant ion quantified the analyte of interest, while the second most abundant ion confirmed the analyte's identity. To improve the ion signal for each analyte, the mass spectrometry was operated in a selected ion monitoring mode, which scanned for specified ions in different groupings.

Table 2. Parameters and conditions of the automated thermal desorption system for gas-phase PAH sampling media (PAH tube) and soot (Filter) analysis .

TD parameters	PAH tube Conditions	Filter Conditions
1st Tube desorption time and temp.	16 min at 320 °C	10 min at 250 °C
2nd Tube desorption time and temp.	-	16 min at 350 °C
Flow path rate and temp.	50 mL/min at 250 °C	
Trap temp.	low: -10 °C, high: 350 °C	
Trap heating rate	24 °C/s	
Trap desorb time	20 min	
Outlet split flow	15 mL/min	

Table 3. Parameters and conditions used on GC/MS for PAH analysis.

GC/MS parameters	Conditions
GC inlet temp.	280 °C, splitless
GC Carrier gas	Helium, 1.7 mL/min
GC Oven	50 °C (hold for 1 min), 50 °C/min to 100 °C (1 min), 5 °C/min to 215 °C (1 min), 5 °C/min to 245 °C (1 min), 5 °C/min to 265 °C (6 min), 5 °C/min to 295 °C (1 min), 5 °C/min to 305 °C (1 min), 5 °C/min to 310 °C (40 min)
MS operation mode	Selected-ion-monitoring (SIM)
MS source temp.	200 °C
MS transfer line temp.	320 °C
Solvent delay	9 min

Calibration curves of the analytes were developed based on a series of dilutions of PAHs in NIST SRM 2260a (A.1). Calibration fits were established from a nominal mass ratio of target to internal standard PAHs to eliminate to account for any analyte losses during the sampling and desorption processes. The PAH TD tubes were spiked with internal standards, NIST SRM 2269 and SRM 2270, before sampling using a Calibration Solution Loading Rig (MARKES International, Llantrisant, UK) with a nitrogen purge flow of 0.100 SLPM for 10 min.

Limit of detection (LOD) and limit of quantification (LOQ) were determined based on the standard deviation of the response, s, and the relative response (response of target analyte/response of internal standard) versus amount ratio (mass of analyte/mass of internal standard), a. The LOD is defined as:

$$LOD = 3.3\frac{s}{a} \tag{1}$$

and the LOQ as

$$LOQ = 10\frac{s}{a} \tag{2}$$

The calibration results are presented in Appendix A.2. A breakthrough test was also performed to determine how much analyte breaks through the sampling tube and the results are shown in Appendix B. Carryover of the analytes from one GC/MS run to another was studied based on the chromatogram area count, and the results are shown in Appendix C.

To determine the concentration of PAHs on soot particulates, small (4 mm in diameter) circular punchouts (5 to 9 count) were taken from the 47 mm filter and inserted in an empty stainless TD tube, which can then be loaded onto the TD system. PAH values obtained from the TD-GC/MS were corrected by multiplying the quotient of the area of the filter and the total area of the punchouts. The same soot-loaded filters were punched out twice to monitor for measurement consistency. Five filters were studied for measurement/analysis duplicate, where the nine punchouts were collected for the first and five for the second set (Fig. 2).

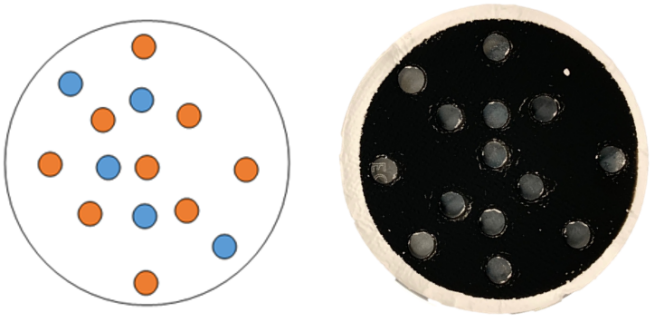

Fig. 2. Typical punch-out location across 47 mm quartz filter (left) and 0.042 SLPM Sample B filter after punch out (right). The first set is in orange, and the second is in blue.

For analysis in the GC/MS, punchout samples were secured in blank TD tubes with quartz fiber wool on both sides to hold filters in place. Before loading the blank TD tubes, the soot punchouts were spiked with internal standards by directly loading the internal standard solution on the soot.

2.4. Determining total PAH concentration

In this work, PAH concentrations and yields are reported as total PAHs, which combine the vapor and particulate phases of the sampling media. The reasoning for reporting PAH concentrations this way is to address the issue of analytes lost from the particle filter during sampling due to volatilization [30]. The fractional difference, defined as the standard deviation of the data set divided by the average value, was used to understand the repeatability of sampling and measurement analysis.

Soot yield, y_s, for each experiment was calculated using Eq. 3:

$$y_s = \frac{m_s}{m_f} \frac{\dot{V}_a + \dot{V}_f}{\dot{V}_{filt}} \tag{3}$$

Here, m_s is the mass difference of filter before and after soot sample collection, and m_f is the total mass of fuel burned during the sampling time. The mass ratio of soot to fuel is multiplied by a volumetric flow correction ratio of the sum of air and fuel, $\dot{V}_a$ and $\dot{V}_f$, into the system to the filter sampling flow, $\dot{V}_{filt}$.

Assuming the sample is collected from a position where the smoke is well-mixed, m_f is determined from Eq. 4 where t is the total time of sampling, P is the pressure, T is the temperature of the room, and $\bar{R}$ is the individual gas constant for propene, (197.6 J/kg K). A constant value for standard temperature and pressure (0 °C and 760 mmHg) was applied to calculate the total fuel mass.

$$m_f = \frac{P\,(\dot{V}_f t)}{\bar{R}\,T} \tag{4}$$

The PAH concentrations are calculated using Eqs. 5 and 6:

$$C_{PAH_{i,TD}} = \frac{m_{PAH_{i,TD}}}{\dot{V}_{TD}\,t} \tag{5}$$

$$C_{PAH_{i,filt}} = \frac{m_{PAH_{i,filt}}\gamma_{filt}}{\dot{V}_{filt}\,t} \tag{6}$$

where the mass detected of analyte, i, in the gas phase, $m_{PAH_{i,TD}}$, and on the filter, $m_{PAH_{i,filt}}$ are divided by the total sample collection volumes. $\dot{V}_{TD}$ is the TD tube sampling flow. For the filter PAH concentration, a surface area correction ratio, γ_{filt}, is multiplied, which is the ratio of the surface area between the filter, d_{filt}, and the punchouts, d_{po}, and the number of punch outs, n_{po} (Eq. 7). It is assumed that soot is deposited on to the filter uniformly.

$$\gamma_{filt} = \frac{d_f^2}{n_{po}\,d_{po}^2} \tag{7}$$

The total PAH concentration, $C_{PAH_{tot}}$, is the summation of all PAH concentrations detected in both TD tube and filter samples (Eq. 18).

$$C_{PAH_{tot}} = \sum_i^{n_{det}} C_{PAH_{i,TD}} + \sum_i^{n_{det}} C_{PAH_{i,filt}} \tag{8}$$

where n_{det} is the number of PAHs detected in an analysis.

The total PAH yield, y_{PAH}, was calculated by combining the total PAH concentration, total volume of flow through the cylinder, and the mass of fuel burned (Eq. 9).

$$y_{PAH} = C_{PAH_{tot}} \left[\frac{(\dot{V}_a + \dot{V}_f)t}{m_f}\right] \tag{9}$$

Appendices D through F presents uncertainty analysis for the reported values. A coverage factor of 2 is applied to the combined uncertainty to produce a 95 % confidence interval. Unless individually calculated, the maximum uncertainty value is applied to all values for a specific variable.

3. Results

3.1. Concentrations of PAHs produced from soot generator

Table 4 lists the total PAH yields and concentrations for each of the five fuel flow conditions studied. One of the samples for 0.030 SLPM propene is reported without the gas-phase value since the sample was compromised by the computer shutting down unexpectedly during the gas chromatography operation. The total PAH concentrations from 0.000 SLPM to 0.050 SLPM of propene fire with 80.00 SLPM of co-flow of air ranged from 1.83 $\mu g/m^3 \pm 1.28\ \mu g/m^3$ to 86.19 $\mu g/m^3 \pm 11.12\ \mu g/m^3$, increasing with fuel flow. Especially for the TD samples, the individual PAHs were detected at the lower end of their calibration range. The total PAH yield ranged from 2.60 $\mu g/g \pm 1.70\ \mu g/g$ to 73.50 $\mu g/g \pm 9.48$ $\mu g/g$ of fuel, also increasing with fuel flow. Since the soot yield is based on the gravimetric mass difference of the filter before and after soot collection, the filters with minimal soot loading fell below the detection limit and consequently did not have soot yields reported in Table 4. The total PAH yields per soot mass for the two higher propene flow conditions are comparable to the values obtained for crude oil; the yields per soot from this study are approximately a fourth of the total PAH yields per soot from crude oil fire on water [27].

Table 4. Soot mass on filter, total PAH concentration (TD, filter, and combined), soot yield, and fuel yield for each fuel flow condition.

Fuel Flow (SLPM)	m_s (mg)	$C_{PAH_{TD}}$ ($\mu g/m^3$)	$C_{PAH_{filt}}$ ($\mu g/m^3$)	$C_{PAH_{tot}}$ ($\mu g/m^3$)	y_s (mg/g fuel)	y_{PAH} (μg/g fuel)
0.000	BDL	0.76 ± 0.32	1.40 ± 1.92	2.16 ± 2.24	-	-
0.030	BDL	0.70 ± 0.02	1.48 ± 0.62	1.83 ± 1.28	-	2.60 ± 1.70
0.038	BDL	0.64 ± 0.12	5.31 ± 1.61	5.96 ± 1.50	-	6.65 ± 3.03
0.042	2.07 ± 0.08	0.66 ± 0.18	33.58 ± 23.78	34.24 ± 23.96	42.10 ± 1.78	34.76 ± 24.34
0.050	3.79 ± 0.12	0.73 ± 0.12	85.46 ± 11.00	86.19 ± 11.12	64.58 ± 2.22	73.50 ± 9.48

The visual soot loading on the filters (Fig. 3) shows the filters turning grey and black for propene flow greater than 0.038 SLPM, darker with higher fuel flow. This correlates with the particle concentration observed; while the total PAH concentration and yields did not increase across 0.000 SLPM and 0.030 SLPM, the concentrations and yields exponentially increased for 0.038 SLPM, 0.042 SLPM, and 0.050 SLPM of propene conditions (Fig. 4). This pattern also correlates well with the particle mass concentration and yield measured by TEOM, which increased exponentially from below the detection limit to 88.30 mg/m^3 and 81.86 mg/g of fuel.

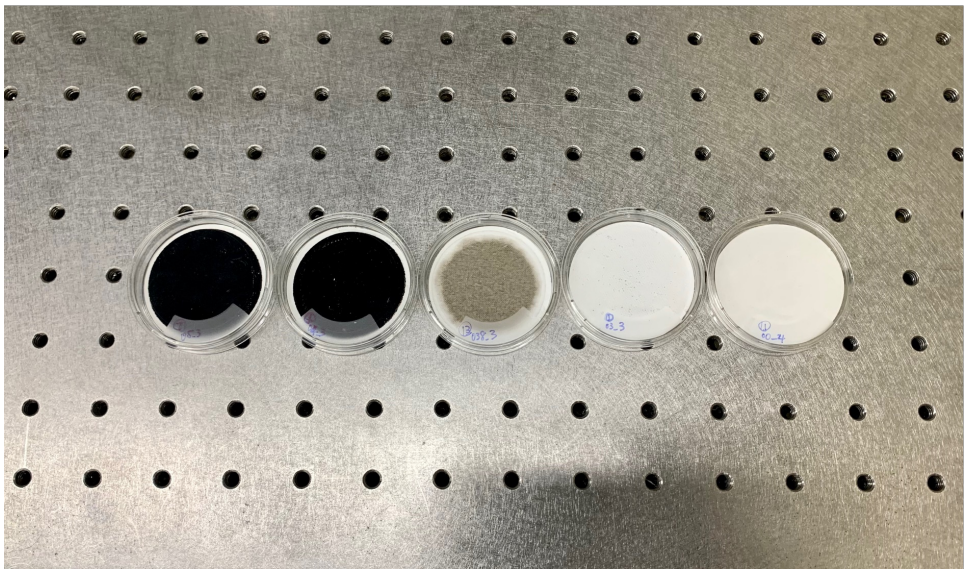

Fig. 3. Soot collected on quartz filters at 0.050 SLPM (3.831 mg ± 0.046 mg), 0.042 SLPM (2.103 mg ± 0.044 mg), 0.038 SLPM (below detection limit), 0.030 SLPM (below detection limit), and zero fuel (below detection limit) from left to right.

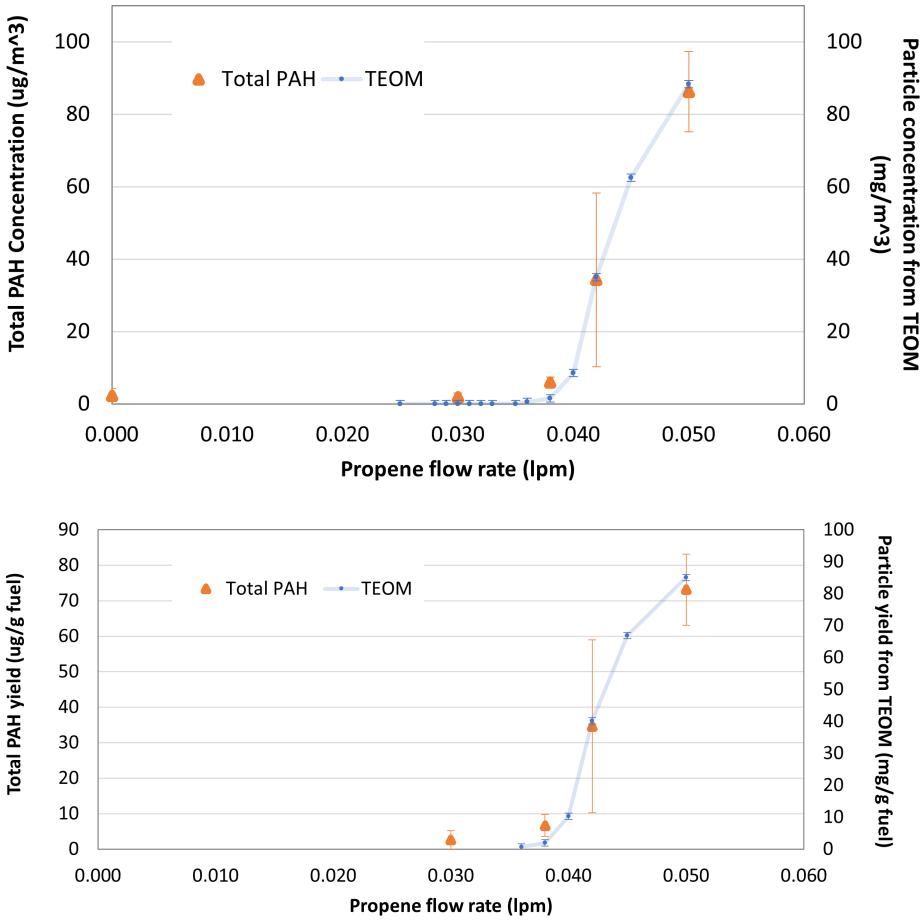

Fig. 4. Total PAH concentration (top) and yield (bottom) averaged across sample duplicates, and particle mass concentration/yield from the tapered element oscillating microbalance (TEOM) for the five fuel flow conditions.

Figure 5 presents the speciated PAH concentrations for each fuel flow condition. PAHs in the soot account for most of the total PAH concentration. The concentration of each measured PAH increased as the fuel flow rate increased in most species. The fraction of PAHs detected in soot increases with the fuel flow, comprising 65 %, 81 %, 89 %, 98 %, and 99 % of the total PAH concentrations for 0.000 SLPM, 0.030 SLPM, 0.038 SLPM, 0.042 SLPM, and 0.050 SLPM fuel flow, respectively. Naphthalene, acenaphthylene, and phenanthrene are the top three PAHs that comprise the bulk of the total PAH concentration, especially for higher fuel flow conditions (0.038 SLPM to 0.050 SLPM). The PAHs with 3 or fewer benzene rings, also referred to as low molecular weight PAHs [35] (naphthalene to anthracene in Table 1), comprise less than 60 % of the total PAH concentration for a fuel flow rate of 0.000 SLPM and 0.030 SLPM, around 70 % at 0.038 SLPM, and 90 % or greater at 0.042 SLPM, and 0.050 SLPM. This may be an indication of the heavier PAHs being consumed to form

more nascent soot in soot-dominant smoke [6], however, further testing is necessary for verification. The large error bars in Figure 5 show test-to-test variability, which may indicate that the propene fire is dynamic even in a controlled environment with controlled fuel flow. Another factor that may affect the speciated fraction may be the timing of sampling, the time since the fuel reached its set point, which may be of interest to investigate further.

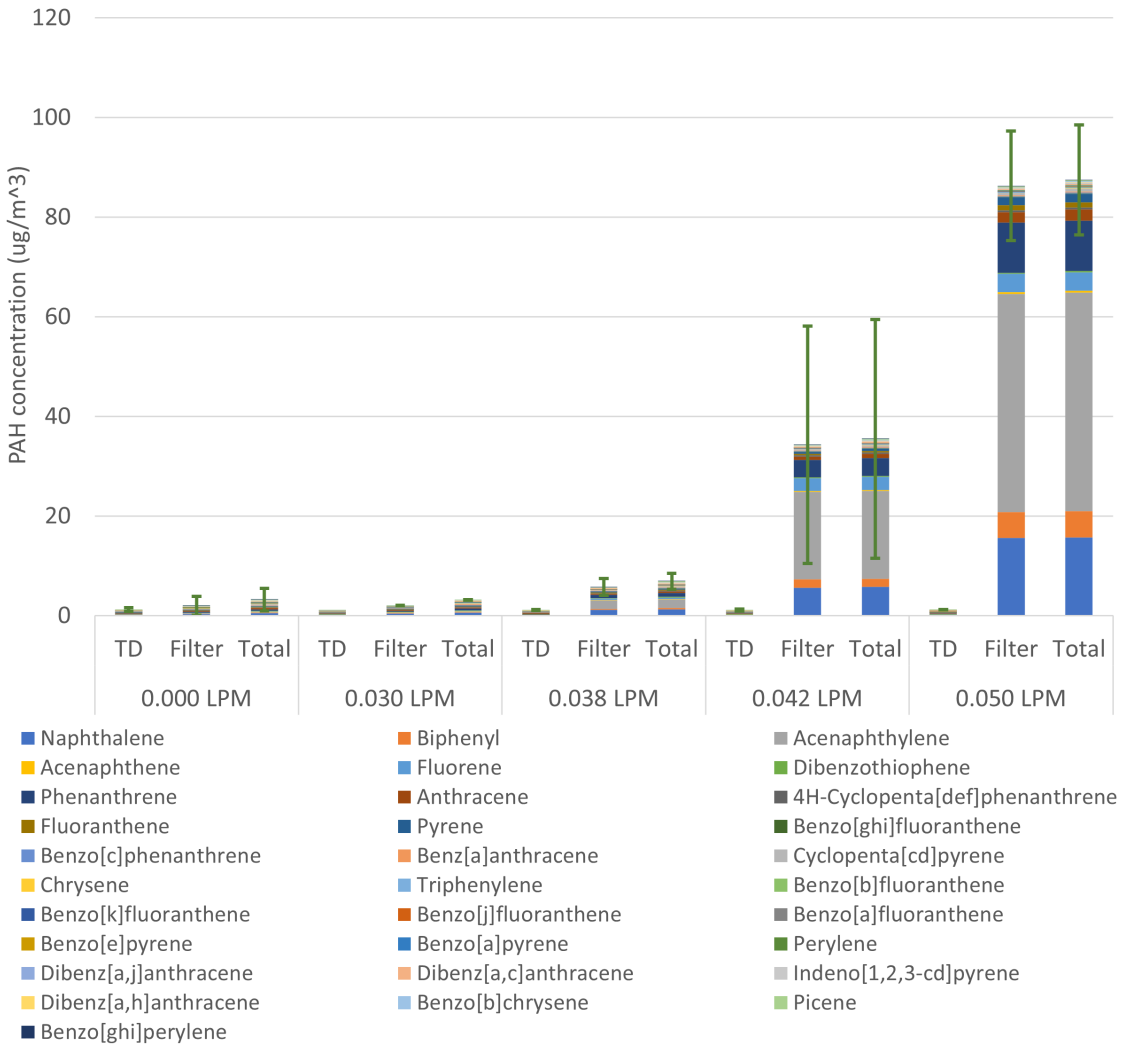

Fig. 5. PAH concentrations separated by gas analysis (TD), filter (soot) analysis, and total which combines concentrations from both TD and filter analyses, averaged across each fuel flow rate (in SLPM).

As observed in Fig. 5, many species of PAH are present in smoke. PAHs from incomplete combustion are often found as complex mixtures and not as a single compound [1]. The EPA lists 16 and 7 priority PAHs that were selected based on their potential exposure and toxicity in humans and other organisms, frequency of occurrence at hazardous waste sites,

and their prevalence and persistence in the environment, and the extent of information available [36]. The total PAH, the sum of 31 analytes, is compared to the sum of the 16 and 7-priority PAHs in Fig. 6. While the priority list is supposed to be representative of different groups of PAHs, analyzing as many PAHs as possible from smoke samples is advantageous since the EPA's 16-PAHs account for 74 % to 92 % of the total of 31 PAHs measured in this study, and the EPA's 7-PAHs account for only 1 % to 19 % of the total PAH.

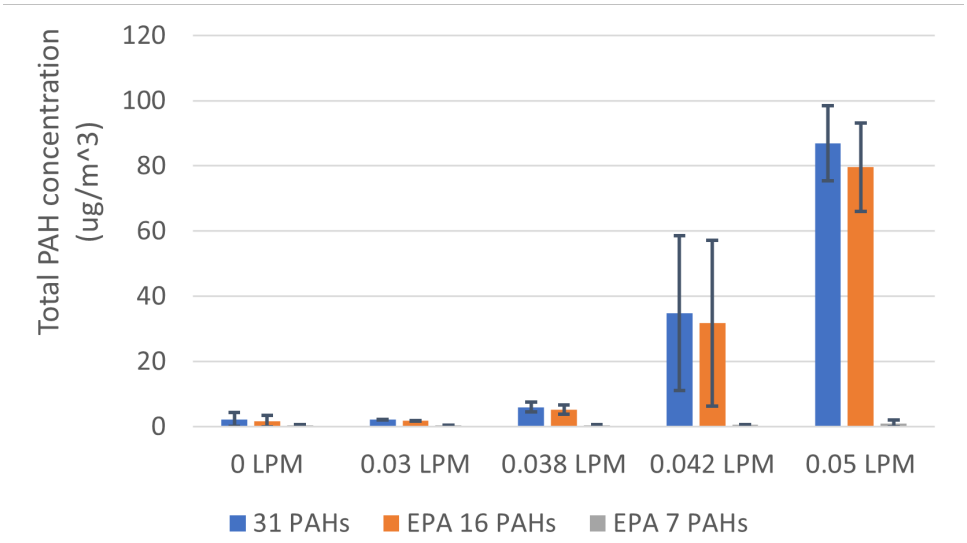

Fig. 6. Sum of all 31 PAHs analyzed (blue), the EPA's 16 priority PAHs (orange), and the EPA's 7 priority PAHs (grey), averaged over each fuel flow rate (in SLPM).

3.2. Consistency of measurement technique

Sample duplicates and measurement duplicates are compared in the following sections. While the composition of the individual PAHs varied from sample to sample, the total PAH concentration is relatively comparable for each fuel condition, with an average of 20 % sample-to-sample variability (Table 5). The gas phase PAH tube analysis is consistent with an 8 % to 21 % variance, although note that all measurements in the gas phase for this study fall within the standard deviation of the zero fuel condition. The filter punch-out method can vary more than tube analysis, ranging from 4 % to 65 %. The significant variance in 0 fuel filters may be due to one of the filters collecting more residual soot in the tubing carried by the co-flow; a few soot particles were visible for one over the other. The variance of the other filters remained below 34 %.

Table 5. Total PAH concentrations ($\mu g/m^3$) averaged across sample duplicates for PAH tube analysis (TD) and soot filter analysis (filter). Gas phase 0.030 SLPM data has one point; therefore not shown. S represents sample-to-sample variability.

	TD	TD	TD	TD	filter	filter	filter	filter	filter
Fuel flow (LPM)	0.000	0.038	0.042	0.050	0.000	0.030	0.038	0.042	0.050
n	3	2	2	2	2	2	2	2	2
Avg.	0.8397	0.6447	0.6626	0.7275	1.401	1.477	5.315	34.20	86.15
S	0.1769	0.0563	0.0940	0.0579	0.915	0.060	0.794	11.78	5.70
S/avg.	21 %	9 %	14 %	8 %	65 %	4 %	15 %	34 %	7 %

The 0.038 SLPM filters used two different tubes: the first set with PAH TD tubes and the second in hollow stainless tubes (Table 6). The data is within 25 %, suggesting that even for filters with the slightest soot loading (where filter mass increase was not observed gravimetrically), $1\ \mu L$ of the internal standards was absorbed by the tube and was able to measure PAH concentrations.

Table 6. Total PAH concentrations ($\mu g/m^3$) for selected five filter samples analyzed with two sets of punchouts. Asterisk for filters analyzed with PAH TD tubes, the rest were analyzed in hollow stainless steel tubes.

Flow rate (LPM)	0.038	0.038	0.042	0.042	0.050
Sample ID	a	b	a	b	a
1st set	5.168*	6.378*	38.43	22.36	83.87
2nd set	7.388	8.950	26.76	21.80	78.77
Avg.	6.278	7.663	32.59	22.08	81.32
S	1.570	1.817	8.26	0.40	3.60
S/avg.	25 %	24 %	25 %	2 %	4 %

The same filters desorbed with TD-GC/MS were spiked again with internal standard and reanalyzed to determine if any PAHs remained after the first desorption process. Table 7 lists the mass of total PAHs detected from the two consecutive desorption processes. Greater than 86 % of the PAHs were desorbed and detected by the first desorption process by TD-GC/MS, with the percentage decreasing with higher soot loading.

Table 7. Total PAH mass detected from soot filter desorption for the second time, reporting the direct mass output from the GC/MS analytical software. Both includes the sum of the output from the first and the second desorption. The quotient of the mass from the second desorption and the total desorbed mass is also presented.

Fuel flow (LPM)	Sample ID	Total PAH $mass_{both}$ (ng)	Total PAH $mass_{2nd\ desorption}$ (ng)	$\frac{\text{Total PAH mass}_{2nd}}{\text{Total PAH mass}_{both}}$
0.042	a	171.7	17.5	10 %
0.042	b	104.1	14.3	14 %
0.050	a	361.9	25.3	7 %
0.050	b	330.7	17.4	5 %

4. Conclusion

The sample collection and analysis method for PAHs without liquid extraction has been presented. The propene laminar flame smoke in the overfire region from this study shows that TD-GC/MS is a viable tool for PAH detection and quantification, using the same analytical method to analyze gas and solid phase PAH samples. The PAHs were predominantly detected in the soot over vapor phase for this experiment; total PAH concentration, soot, and fuel yields followed a similar trend as particle concentration/yield, increasing as the flame transitioned from non-sooting to sooting above its smoke point. We hope to apply this method to other fuel sources to gather more PAH yields, which have not been studied as well as other combustion gasses. These PAH yields can help predict exposure concentrations downstream of the fire and can potentially provide further insight into understanding soot formation.

5. References

[1] ATSDR PUBLIC HEALTH STATEMENT POLYCYCLIC AROMATIC HYDROCARBONS (PAHs). Available at https://www.atsdr.cdc.gov/ToxProfiles/tp69-c1-b.pdf.

[2] Xu P, Liu B, Chen H, Wang H, Guo X, Yuan J (2024) Pahs as environmental pollutants and their neurotoxic effects. *Comparative Biochemistry and Physiology Part C: Toxicology & Pharmacology* :109975.

[3] International Ageny for Research and Cancer IARC Monographs on the Identification of Carcinogenic Hazards to Humans, List of Classifications. Available at https://monographs.iarc.who.int/list-of-classifications.

[4] Zelinkova Z, Wenzl T The Occurrence of 16 EPA PAHs in Food – A Review 35(2-4):248–284. https://doi.org/10.1080/10406638.2014.918550. Available at https://www.tandfonline.com/doi/full/10.1080/10406638.2014.918550

[5] Tsiodra I, Grivas G, Bougiatioti A, Tavernaraki K, Parinos C, Paraskevopoulou D, Papoutsidaki K, Tsagkaraki M, Kozonaki FA, Oikonomou K, Nenes A, Mihalopoulos N (2024) Source apportionment of particle-bound polycyclic aromatic hydrocarbons (PAHs), oxygenated PAHs (OPAHs), and their associated long-term health risks in a major European city. *Science of The Total Environment* 951:175416. https://doi.org/10.1016/j.scitotenv.2024.175416

[6] Richter H, Howard JB (2000) Formation of polycyclic aromatic hydrocarbons and their growth to soot—a review of chemical reaction pathways. *Progress in Energy and Combustion science* 26(4-6):565–608.

[7] Homann K (1985) Formation of large molecules, particulates and ions in premixed hydrocarbon flames; progress and unresolved questions. *Symposium (International) on Combustion*, Vol. 20, pp 857–870.

[8] Howard JB (1991) Carbon addition and oxidation reactions in heterogeneous combustion and soot formation. *Symposium (International) on Combustion*, Vol. 23, pp 1107–1127.

[9] Frenklach M, Wang H (1991) Detailed modeling of soot particle nucleation and growth. *Symposium (International) on combustion*, Vol. 23, pp 1559–1566.

[10] Benish TG, Lafeur AL, Taghiadeh K, Howard JB (1996) C2h2 and pah as soot growth reactants in premixed c2h4-air flames. *Symposium (International) on Combustion* (Elsevier), Vol. 26, pp 2319–2326.

[11] Wang H, Frenklach M (1997) A detailed kinetic modeling study of aromatics formation in laminar premixed acetylene and ethylene flames. *Combustion and flame* 110(1-2):173–221.

[12] Kazakov A, Frenklach M (1998) On the relative contribution of acetylene and aromatics to soot particle surface growth. *Combustion and flame* 112(1-2):270–274.

[13] D'Anna A, Violi A (1998) A kinetic model for the formation of aromatic hydrocarbons in premixed laminar flames. *Symposium (International) on Combustion*, Vol. 27, pp 425–433.

[14] Wang H (2011) Formation of nascent soot and other condensed-phase materials in flames. *Proceedings of the Combustion Institute* 33(1):41–67.

[15] Desgroux P, Mercier X, Thomson KA (2013) Study of the formation of soot and its precursors in flames using optical diagnostics. *Proceedings of the Combustion Institute* 34(1):1713–1738.

[16] Chernov V, Thomson MJ, Dworkin SB, Slavinskaya NA, Riedel U (2014) Soot formation with c1 and c2 fuels using an improved chemical mechanism for pah growth. *Combustion and Flame* 161(2):592–601.

[17] An Yz, Li X, Teng Sp, Wang K, Pei Yq, Qin J, Zhao H (2016) Development of a soot particle model with pahs as precursors through simulations and experiments. *Fuel* 179:246–257.

[18] Liu P, Li Z, Roberts WL (2019) The growth of pahs and soot in the post-flame region. *Proceedings of the Combustion Institute* 37(1):977–984.

[19] Nobili A, Maffei LP, Baggioli A, Pelucchi M, Cuoci A, Cavallotti C, Faravelli T (2022) On the radical behavior of large polycyclic aromatic hydrocarbons in soot formation and oxidation. *Combustion and Flame* 235:111692.

[20] Jensen D (1974) Prediction of soot formation rates: a new approach. *Proceedings of the Royal Society of London A Mathematical and Physical Sciences* 338(1614):375–396.

[21] D'Anna A, D'Alessio A, Minutolo P (1994) Spectroscopic and chemical characterization of soot inception processes in premixed laminar flames at atmospheric pressure. *Soot formation in combustion: mechanisms and models* (Springer), pp 83–103.

[22] Cain J, Laskin A, Kholghy MR, Thomson MJ, Wang H (2014) Molecular characterization of organic content of soot along the centerline of a coflow diffusion flame. *Physical Chemistry Chemical Physics* 16(47):25862–25875.

[23] Sabbah H, Commodo M, Picca F, De Falco G, Minutolo P, D'Anna A, Joblin C (2021) Molecular content of nascent soot: Family characterization using two-step laser desorption laser ionization mass spectrometry. *Proceedings of the Combustion Institute* 38(1):1241–1248.

[24] Jacobson RS, Korte AR, Vertes A, Miller JH (2020) The molecular composition of soot. *Angewandte Chemie* 132(11):4514–4520.

[25] Adamson BA, Skeen SA, Ahmed M, Hansen N (2020) Nucleation of soot: experimental assessment of the role of polycyclic aromatic hydrocarbon (pah) dimers. *Zeitschrift für Physikalische Chemie* 234(7-9):1295–1310.

[26] Shao C, Wang Q, Zhang W, Bennett A, Li Y, Guo J, Im HG, Roberts WL, Violi A, Sarathy SM (2023) Elucidating the polycyclic aromatic hydrocarbons involved in soot inception. *Communications Chemistry* 6(1):223.

[27] Benner Jr BA, Bryner NP, Wise SA, Mulholland GW, Lao RC, Fingas MF (1990) Polycyclic aromatic hydrocarbon emissions from the combustion of crude oil on water. *Environmental science & technology* 24(9):1418–1427.

[28] Claessens H, Rhemrev M, Wevers J, Janssen A, Brasser L (1991) Comparison of extraction methods for the determination of polycyclic aromatic hydrocarbons in soot samples. *Chromatographia* 31:569–574.
[29] Jonker MT, Koelmans AA (2002) Extraction of polycyclic aromatic hydrocarbons from soot and sediment: solvent evaluation and implications for sorption mechanism. *Environmental science & technology* 36(19):4107–4113.
[30] US EPA Compendium Method TO-13A Determination of Polycyclic Aromatic Hydrocarbons (PAHs) in Ambient Air Using Gas Chromatography/Mass Spectrometry (GC/MS). Available at https://www.epa.gov/sites/default/files/2019-11/documents/to-13arr.pdf.
[31] Cleary TG, Mulholland GW, Ives LK, Fletcher RA, Gentry J (1992) Ultrafine combustion aerosol generator. *Aerosol science and technology* 16(3):166–170.
[32] Mensch AE, Cleary TG (2019) Measurements and predictions of thermophoretic soot deposition. *International journal of heat and mass transfer* 143:118444.
[33] Choi MY, Mulholland GW, Hamins A, Kashiwagi T (1995) Comparisons of the soot volume fraction using gravimetric and light extinction techniques. *Combustion and Flame* 102(1-2):161–169.
[34] Falkenstein-Smith R, Harris K, Sung K, Liang T, Hamins A (2022) A calibration and sampling technique for quantifying the chemical structure in fires using gc/msd analysis. *Fire and Materials* 46(1):3–11.
[35] Takam P, Schäffer A, Laovitthayanggoon S, Charerntantanakul W, Sillapawattana P (2024) Toxic effect of polycyclic aromatic hydrocarbons (pahs) on co-culture model of human alveolar epithelial cells (a549) and macrophages (thp-1). *Environmental Sciences Europe* 36(1):176.
[36] ATSDR (2005) Toxicology profile for polyaromatic hydrocarbons.

Appendix A. Calibration and Limits of Detection and Quantification

Appendix A.1. Mass of PAH calibrants and internal standards

Table 8. Nominal mass of target and internal standard PAHs in calibration curve used for determination of limits of detection and quantification

Compound	Cal. Std. 0 (ng)	Cal. Std. 1 (ng)	Cal. Std. 2 (ng)	Cal. Std. 3 (ng)	Cal. Std. 4 (ng)	Cal. Std. 5 (ng)
Biphenyl-d10	4.44E-01	4.44E-01	4.44E-01	4.44E-01	4.44E-01	4.44E-01
Phenanthrene-d10	2.11E+00	2.11E+00	2.11E+00	2.11E+00	2.11E+00	2.11E+00
Fluoranthene-d10	3.55E+00	3.55E+00	3.55E+00	3.55E+00	3.55E+00	3.55E+00
Benz[a]anthracene-d12	2.15E+00	2.15E+00	2.15E+00	2.15E+00	2.15E+00	2.15E+00
Dibenz[a,h]anthracene-d14	4.23E-01	4.23E-01	4.23E-01	4.23E-01	4.23E-01	4.23E-01
Naphthalene-d8	4.33E+00	4.33E+00	4.33E+00	4.33E+00	4.33E+00	4.33E+00
Acenaphthene-d10	4.28E-01	4.28E-01	4.28E-01	4.28E-01	4.28E-01	4.28E-01
Pyrene-d10	4.19E+00	4.19E+00	4.19E+00	4.19E+00	4.19E+00	4.19E+00
Benzo[a]pyrene-d12	2.10E+00	2.10E+00	2.10E+00	2.10E+00	2.10E+00	2.10E+00
Perylene-d12	1.68E+00	1.68E+00	1.68E+00	1.68E+00	1.68E+00	1.68E+00
Benzo[ghi]perylene-d12	1.99E+00	1.99E+00	1.99E+00	1.99E+00	1.99E+00	1.99E+00
Naphthalene	0.00E+00	5.78E-03	3.64E-01	2.07E+00	4.13E+00	1.69E+01
Biphenyl	0.00E+00	3.53E-03	1.85E-01	1.03E+00	2.03E+00	9.17E+00
Acenaphthylene	0.00E+00	3.16E-03	1.99E-01	1.13E+00	2.26E+00	9.23E+00
Acenaphthene	0.00E+00	2.80E-03	1.77E-01	1.00E+00	2.00E+00	8.18E+00
Fluorene	0.00E+00	2.38E-03	1.50E-01	8.52E-01	1.70E+00	6.94E+00
Dibenzothiophene	0.00E+00	2.76E-03	1.45E-01	8.04E-01	1.59E+00	7.18E+00
Phenanthrene	0.00E+00	7.29E-03	3.82E-01	2.12E+00	4.18E+00	1.89E+01
Anthracene	0.00E+00	2.35E-03	1.23E-01	6.84E-01	1.35E+00	6.11E+00
4H-Cyclopenta[def]phenanthrene	0.00E+00	1.46E-03	7.65E-02	4.25E-01	8.38E-01	3.79E+00
Fluoranthene	0.00E+00	5.24E-03	2.74E-01	1.52E+00	3.01E+00	1.36E+01
Pyrene	0.00E+00	4.52E-03	2.85E-01	1.62E+00	3.23E+00	1.32E+01
Benzo[ghi]fluoranthene	0.00E+00	2.15E-03	1.13E-01	6.25E-01	1.23E+00	5.58E+00
Cyclopenta[cd]pyrene	0.00E+00	1.23E-03	6.46E-02	3.58E-01	7.07E-01	3.20E+00
Benzo[c]phenanthrene	0.00E+00	2.90E-03	1.52E-01	8.44E-01	1.66E+00	7.53E+00
Benz[a]anthracene	0.00E+00	2.78E-03	1.46E-01	8.08E-01	1.59E+00	7.22E+00
Chrysene	0.00E+00	2.91E-03	1.52E-01	8.46E-01	1.67E+00	7.55E+00
Triphenylene	0.00E+00	2.59E-03	1.36E-01	7.54E-01	1.49E+00	6.74E+00
Benzo[b]fluoranthene	0.00E+00	3.97E-03	2.50E-01	1.42E+00	2.84E+00	1.16E+01
Benzo[j]fluoranthene	0.00E+00	2.09E-03	1.32E-01	7.50E-01	1.50E+00	6.11E+00
Benzo[k]fluoranthene	0.00E+00	1.74E-03	1.10E-01	6.23E-01	1.24E+00	5.08E+00
Benzo[a]fluoranthene	0.00E+00	1.15E-03	7.26E-02	4.12E-01	8.23E-01	3.36E+00
Benzo[e]pyrene	0.00E+00	2.30E-03	1.45E-01	8.25E-01	1.65E+00	6.72E+00
Benzo[a]pyrene	0.00E+00	2.38E-03	1.50E-01	8.52E-01	1.70E+00	6.94E+00
Perylene	0.00E+00	2.24E-03	1.41E-01	8.01E-01	1.60E+00	6.53E+00
Indeno[1,2,3-cd]pyrene	0.00E+00	2.79E-03	1.46E-01	8.10E-01	1.60E+00	7.23E+00
Benzo[ghi]perylene	0.00E+00	2.86E-03	1.81E-01	1.03E+00	2.05E+00	8.36E+00
Dibenz[a,h]anthracene	0.00E+00	2.87E-03	1.50E-01	8.34E-01	1.64E+00	7.45E+00
Dibenz[a,j]anthracene	0.00E+00	2.86E-03	1.50E-01	8.31E-01	1.64E+00	7.42E+00
Dibenz[a,c]anthracene	0.00E+00	1.83E-03	9.60E-02	5.33E-01	1.05E+00	4.76E+00
Picene	0.00E+00	1.65E-03	1.04E-01	5.89E-01	1.18E+00	4.80E+00
Benzo[b]chrysene	0.00E+00	2.07E-03	1.30E-01	7.40E-01	1.48E+00	6.03E+00
Anthanthrene	0.00E+00	1.11E-03	7.03E-02	3.99E-01	7.96E-01	3.25E+00
Coronene	0.00E+00	1.14E-03	7.19E-02	4.08E-01	8.14E-01	3.32E+00
Dibenzo[b,k]fluoranthene	0.00E+00	8.32E-04	5.24E-02	2.98E-01	5.94E-01	2.43E+00
Dibenzo[a,e]pyrene	0.00E+00	1.15E-03	7.26E-02	4.12E-01	8.22E-01	3.36E+00

Appendix A.2. LOD and LOQ

Table 9. Limit of detection (LOD) and limit of quantification (LOQ) for the PAH analytes with R^2 values for their calibration curves

Analyte	LOD (ng)	LOQ (ng)	R^2
Naphthalene	0.065	0.197	0.9999
Biphenyl	0.006	0.017	0.9999
Acenaphthylene	0.011	0.034	0.9988
Acenaphthene	0.010	0.031	0.9997
Fluorene	0.010	0.031	0.9993
Dibenzothiophene	0.142	0.429	0.9968
Phenanthrene	0.056	0.171	0.9989
Anthracene	0.198	0.601	0.9905
4H-Cyclopenta[def]phenanthrene	0.137	0.415	0.9966
Fluoranthene	0.069	0.210	0.9995
Pyrene	0.094	0.284	0.9995
Benzo[ghi]fluoranthene	0.021	0.065	0.9985
Benzo[c]phenanthrene	0.044	0.133	0.9985
Benz[a]anthracene	0.038	0.115	0.9984
Cyclopenta[cd]pyrene	0.292	0.884	0.9887
Chrysene	0.039	0.119	0.9983
Triphenylene	0.030	0.090	0.9986
Benzo[b]fluoranthene	0.074	0.223	0.9981
Benzo[k]fluoranthene	0.064	0.193	0.9986
Benzo[j]fluoranthene	0.019	0.058	0.9999
Benzo[a]fluoranthene	0.110	0.334	0.9978
Benzo[e]pyrene	0.053	0.160	0.9991
Benzo[a]pyrene	0.027	0.081	0.9998
Perylene	0.034	0.103	0.9996
Dibenz[a,j]anthracene	0.009	0.027	0.9996
Dibenz[a,c]anthracene	0.049	0.147	0.9920
Indeno[1,2,3-cd]pyrene	0.016	0.049	0.9978
Dibenz[a,h]anthracene	0.008	0.024	0.9995
Benzo[b]chrysene	0.129	0.390	0.9995
Picene	0.144	0.436	0.9992
Benzo[ghi]perylene	0.020	0.061	0.9999
Anthanthrene	0.385	1.166	0.9961
Dibenzo[b,k]fluoranthene	0.570	1.726	0.9975
Dibenzo[a,e]pyrene	1.961	5.943	0.9942
Coronene	0.556	1.684	0.9884

Appendix B. Breakthrough

Table 10. Breakthrough to subsequent (2nd and 3rd) tubes based on area count of PAH analytes with a known amount (1 µL of Cal. Std. 4) in the first sorbent tube, relative percentage (%) based on the amount detected in the first tube. The average (Avg.) and the standard deviation (SD) of the breakthrough percentage onto the second and third tubes are also listed.

	Data 1		Data 2		Data 3		2nd tube		3rd tube	
Tube number	2nd (%)	3rd (%)	2nd (%)	3rd (%)	2nd (%)	3rd (%)	Avg. (%)	SD (%)	Avg. (%)	SD (%)
Naphthalene	4.00	4.00	4.63	0.00	7.90	3.49	5.51	2.09	2.50	2.18
Biphenyl	29.0	13.2	3.62	0.00	3.92	2.77	12.2	14.6	5.32	6.96
Acenaphthylene	0.80	0.00	0.15	0.00	0.41	0.47	0.45	0.33	0.16	0.27
Acenaphthene	0.70	1.10	0.00	0.00	0.03	0.19	0.24	0.40	0.43	0.59
Fluorene	2.30	3.40	1.06	0.00	1.86	2.28	1.74	0.63	1.89	1.73
Dibenzothiophene	0.90	0.00	0.08	0.00	0.39	0.53	0.46	0.41	0.18	0.31
Phenanthrene	0.00	0.00	0.91	0.00	1.11	1.31	0.68	0.59	0.44	0.76
Anthracene	0.60	0.40	0.00	0.00	0.00	0.00	0.20	0.35	0.13	0.23
4H-Cyclopenta[def]phenanthrene	0.00	0.00	0.14	0.00	0.33	0.38	0.16	0.17	0.13	0.22
Fluoranthene	0.00	0.00	0.18	0.00	0.33	0.70	0.17	0.16	0.23	0.40
Pyrene	0.00	0.00	0.00	0.00	0.00	0.24	0.00	0.00	0.08	0.14
Benzo[ghi]fluoranthene	0.00	0.00	0.00	0.00	0.00	0.42	0.00	0.00	0.14	0.24
Benzo[c]phenanthrene	0.10	0.00	0.00	0.00	0.00	0.36	0.03	0.06	0.12	0.21
Benz[a]anthracene	0.00	0.00	0.14	0.00	0.34	0.98	0.16	0.17	0.33	0.56
Cyclopenta[cd]pyrene	0.00	0.00	0.00	0.00	0.00	0.00	0.00	0.00	0.00	0.00
Chrysene	0.00	0.00	0.00	0.00	0.00	0.85	0.00	0.00	0.28	0.49
Triphenylene	0.10	0.00	0.89	0.00	0.00	2.57	0.33	0.49	0.86	1.48
Benzo[b]fluoranthene	1.20	0.00	0.21	0.00	0.79	2.24	0.73	0.50	0.75	1.29
Benzo[k]fluoranthene	1.70	0.00	0.00	0.00	0.00	0.00	0.57	0.98	0.00	0.00
Benzo[j]fluoranthene	0.80	0.00	0.44	0.00	0.97	2.20	0.74	0.27	0.73	1.27
Benzo[a]fluoranthene	0.60	0.00	0.00	0.00	0.10	1.10	0.23	0.32	0.37	0.63
Benzo[e]pyrene	0.70	0.00	0.00	0.00	0.00	1.43	0.23	0.40	0.48	0.82
Benzo[a]pyrene	1.60	0.00	0.00	0.00	0.00	2.17	0.53	0.92	0.72	1.25
Perylene	1.00	0.00	0.00	0.00	0.00	1.31	0.33	0.58	0.44	0.76
Dibenz[a,j]anthracene	7.50	0.00	0.00	0.00	1.74	5.75	3.08	3.93	1.92	3.32
Dibenz[a,c]anthracene	9.40	0.00	0.00	0.00	3.10	6.09	4.17	4.79	2.03	3.52
Indeno[1,2,3-cd]pyrene	11.6	0.00	0.00	0.00	0.00	6.10	3.87	6.70	2.03	3.52
Dibenz[a,h]anthracene	14.7	0.00	1.57	0.00	3.72	9.67	6.66	7.04	3.22	5.58
Benzo[b]chrysene	11.4	0.00	0.00	0.00	0.15	6.42	3.85	6.54	2.14	3.71
Picene	10.2	0.00	0.00	0.00	0.79	6.52	3.66	5.67	2.17	3.76
Benzo[ghi]perylene	9.50	0.00	0.00	0.00	0.00	3.24	3.17	5.48	1.08	1.87

Appendix C. Carryover

Table 11. Carryover in % based on the area count ratio of the subsequent run with an empty tube and the PAH analytes with known amount loaded onto a PAH TD tube: 1 µL of Cal. Std. 2, Cal. Std. 4, and Cal. Std. 5. The average of the three results and its standard deviation are also listed.

Analyte	Cal. Std. 2 (rel.%)	Cal. Std. 4 (rel.%)	Cal Std. 5 (rel.%)	Average (rel.%)	Std. Dev. (rel.%)
Naphthalene	0.00	0.40	0.10	0.17	0.21
Biphenyl	0.00	0.70	0.51	0.40	0.36
Acenaphthylene	0.00	0.30	0.30	0.20	0.17
Acenaphthene	0.00	0.30	0.32	0.21	0.18
Fluorene	1.52	0.30	0.36	0.72	0.69
Dibenzothiophene	1.78	0.60	0.33	0.90	0.77
Phenanthrene	1.31	0.20	0.13	0.54	0.66
Anthracene	5.44	1.90	1.40	2.91	2.20
4H-Cyclopenta[def]phenanthrene	0.00	0.20	0.21	0.14	0.12
Fluoranthene	0.00	0.30	0.33	0.21	0.18
Pyrene	0.00	0.30	0.34	0.21	0.19
Benzo[ghi]fluoranthene	0.00	0.40	0.69	0.36	0.35
Benzo[c]phenanthrene	0.00	0.30	0.72	0.34	0.36
Benz[a]anthracene	0.00	0.40	0.54	0.31	0.28
Cyclopenta[cd]pyrene	0.00	7.70	0.00	2.57	4.45
Chrysene	0.04	0.50	0.52	0.35	0.27
Triphenylene	0.04	1.00	0.50	0.51	0.48
Benzo[b]fluoranthene	0.00	0.40	0.89	0.43	0.44
Benzo[k]fluoranthene	0.00	12.4	2.44	4.95	6.57
Benzo[j]fluoranthene	0.00	3.00	0.00	1.00	1.73
Benzo[a]fluoranthene	0.00	1.50	0.86	0.79	0.75
Benzo[e]pyrene	0.00	1.20	1.72	0.97	0.88
Benzo[a]pyrene	0.00	0.70	1.16	0.62	0.59
Perylene	0.00	0.70	1.50	0.73	0.75
Dibenz[a,j]anthracene	0.00	1.90	2.14	1.35	1.17
Dibenz[a,c]anthracene	0.00	1.10	1.25	0.78	0.68
Indeno[1,2,3-cd]pyrene	0.00	2.10	2.07	1.39	1.21
Dibenz[a,h]anthracene	0.00	3.40	0.86	1.42	1.77
Benzo[b]chrysene	0.00	1.50	1.74	1.08	0.94
Picene	0.00	2.00	1.22	1.07	1.01
Benzo[ghi]perylene	0.00	2.40	3.03	1.81	1.60

Appendix D. Uncertainty of Soot Yield

Soot yield, y_s, for each experiment was calculated using Eq. 10:

$$y_s = \frac{m_s}{m_f}\frac{\dot{V}_{sys}}{\dot{V}_{filt}} \quad ; \quad \dot{V}_{sys} = \dot{V}_a + \dot{V}_f \tag{10}$$

where m_s is the mass of soot collected, and m_f is the total mass of fuel burned during the sampling time, $\dot{V}_{filt}$ is the filter sampling flow rate, and $\dot{V}_a$ and $\dot{V}_f$ are volumetric flow rates of air and fuel into the system and combining the two makes the total flow through the system ($\dot{V}_{sys}$). The uncertainty of the soot yield is estimated using propagation of uncertainty:

$$u_{y_s} = \sqrt{\left(\frac{\partial y_s}{\partial m_s}u_{m_s}\right)^2 + \left(\frac{\partial y_s}{\partial m_f}u_{m_f}\right)^2 + \left(\frac{\partial y_s}{\partial \dot{V}_{filt}}u_{\dot{V}_{filt}}\right)^2 + \left(\frac{\partial y_s}{\partial \dot{V}_{sys}}u_{\dot{V}_{sys}}\right)^2} \tag{11}$$

Appendix D.1. Mass of soot

The mass of soot is determined from the difference in mass of the desiccated quartz filter before and at least 24 h after each experiment. The Type A evaluation of standard uncertainty of the mass of soot, s_{m_s}, is taken as the standard deviation of the measurements, m_s, sampled three times before and after each experiment. The Type B evaluation of uncertainty, u_{inst}, is determined from the instrumentation error sources of the scale and is found to be 1 % of the reading. The Type A evaluation of uncertainty dominates; thus, the standard uncertainty is approximately the standard deviation of the multiple measurements:

$$u_{m_s} \approx s_{m_s} \tag{12}$$

Appendix D.2. Mass of fuel

The mass of fuel is calculated from Eq. 4, and the uncertainty of the mass of fuel is:

$$u_{m_f} = \sqrt{\left(\frac{\partial m_f}{\partial \dot{V}_f}u_{\dot{V}_f}\right)^2} \tag{13}$$

It is simplified to be based on the uncertainty of the volumetric fuel flow, as all other parameters in Eq. 4 are assumed to be fixed. The Type A evaluation of uncertainty of the volumetric fuel flow is the standard deviation of the fuel flow reading on the mass flow controller. The Type B evaluation of uncertainty, u_{inst}, is the uncertainty of the mass flow controller and is found to be 5 % of the reading. The Type B evaluation of uncertainty dominates; thus, the standard uncertainty is approximately the uncertainty of the mass flow controller.

$$u_{\dot{V}_f} \approx u_{inst} \tag{14}$$

Appendix D.3. Volumetric filter sampling flow rate

Similar to the uncertainty of the volumetric fuel flow, Type B evaluation of uncertainty dominates for the uncertainty of the volumetric filter sampling flow rate, which is also at 5 % of the reading. Therefore, the uncertainty of the volumetric flow rate through the filter is approximately the uncertainty of the pump.

$$u_{\dot{V}_{\text{filt}}} \approx u_{\text{inst}} \tag{15}$$

Appendix D.4. Volumetric flow through the system

$\dot{V}_{\text{sys}}$ is the sum of $\dot{V}_{\text{a}}$ and $\dot{V}_{\text{f}}$. The propagation of uncertainty for the volumetric flow through the system is:

$$u_{\dot{V}_{\text{sys}}} = \sqrt{\left(\frac{\partial \dot{V}_{\text{sys}}}{\partial \dot{V}_{\text{f}}} u_{\dot{V}_{\text{f}}}\right)^2 + \left(\frac{\partial \dot{V}_{\text{sys}}}{\partial \dot{V}_{\text{a}}} u_{\dot{V}_{\text{a}}}\right)^2} \tag{16}$$

Here, $\dot{V}_{\text{f}}$ is much smaller than $\dot{V}_{\text{a}}$. $\dot{V}_{\text{f}}$ is negligible, therefore $u_{\dot{V}_{\text{sys}}}$ is approximately $u_{\dot{V}_{\text{a}}}$. Also for $u_{\dot{V}_{\text{a}}}$, the Type B evaluation of standard uncertainty is dominating, therefore, $u_{\dot{V}_{\text{a}}}$ is approximately the instrument uncertainty of the mass flow controller, which is 5 % of the reading.

$$u_{\dot{V}_{\text{sys}}} \approx u_{\text{inst}} \tag{17}$$

Appendix E. Uncertainty of the Individual and Total Concentration of PAHs

Concentration for the total PAH, $C_{\mathrm{PAH_{tot}}}$, which is the summation of all identified PAHs for each experiment was calculated using Eq. 18:

$$C_{\mathrm{PAH_{tot}}} = \sum_{i}^{\mathrm{n_{det}}} C_{\mathrm{PAH}_{i,\mathrm{TD}}} + \sum_{i}^{\mathrm{n_{det}}} C_{\mathrm{PAH}_{i,\mathrm{filt}}} \tag{18}$$

where $C_{\mathrm{PAH}_{i,\mathrm{TD}}}$ is the concentration of a specific PAH (i) detected by the TD tube analysis, $C_{\mathrm{PAH}_{i,\mathrm{filt}}}$ is the concentration of a specific PAH detected by the filter analysis, and n_{det} is the number of detected PAHs. The uncertainty of the total PAH concentration is estimated using propagation of uncertainty:

$$u_{C_{\mathrm{PAH_{tot}}}} = \sqrt{\sum_{i}^{\mathrm{n_{det}}} \left(\frac{\partial C_{\mathrm{PAH_{tot}}}}{\partial C_{\mathrm{PAH}_{i,\mathrm{TD}}}} u_{C_{\mathrm{PAH}_{i,\mathrm{TD}}}} \right)^2 + \sum_{i}^{\mathrm{n_{det}}} \left(\frac{\partial C_{\mathrm{PAH_{tot}}}}{\partial C_{\mathrm{PAH}_{i,\mathrm{filt}}}} u_{C_{\mathrm{PAH}_{i,\mathrm{filt}}}} \right)^2} \tag{19}$$

which ends up being the combined uncertainty associated with the uncertainty of all the identified species for both TD tube and filter sampling methods.
Concentrations of individual PAH obtained from TD tube and filter analyses are in Eqs. 5 and 6. The uncertainty of PAH concentration obtained from TD tubes, $u_{C_{\mathrm{PAH}_{i,\mathrm{TD}}}}$, is estimated by performing the law of propagation of uncertainty on Eq. 5:

$$u_{C_{\mathrm{PAH}_{i,\mathrm{TD}}}} = \sqrt{\left(\frac{\partial C_{\mathrm{PAH}_{i,\mathrm{TD}}}}{\partial m_{\mathrm{PAH_{i,TD}}}} u_{m_{\mathrm{PAH_{i,TD}}}} \right)^2 + \left(\frac{\partial C_{\mathrm{PAH_{i,TD}}}}{\partial \dot{V}_{\mathrm{TD}}} u_{\dot{V}_{\mathrm{TD}}} \right)^2} \tag{20}$$

where $u_{m_{\mathrm{PAH_{i,TD}}}}$ is the uncertainty of PAH mass detected by GC/MS from filter samples and $u_{\dot{V}_{\mathrm{TD}}}$ is the uncertainty of the volumetric flow through the TD tube samples.
The uncertainty of PAH concentration obtained from soot collected on filters, $u_{C_{\mathrm{PAH}_{i,\mathrm{filt}}}}$, is estimated by performing the law of propagation of uncertainty on Eq. 6:

$$u_{C_{\mathrm{PAH}_{i,\mathrm{filt}}}} = \sqrt{\left(\frac{\partial C_{\mathrm{PAH}_{i,\mathrm{filt}}}}{\partial m_{\mathrm{PAH_{i,filt}}}} u_{m_{\mathrm{PAH_{i,filt}}}} \right)^2 + \left(\frac{\partial C_{\mathrm{PAH_{i,filt}}}}{\partial \dot{V}_{\mathrm{filt}}} u_{\dot{V}_{\mathrm{filt}}} \right)^2 + \left(\frac{\partial C_{\mathrm{PAH_{i,filt}}}}{\partial \gamma_{\mathrm{filt}}} u_{\gamma_{\mathrm{filt}}} \right)^2} \tag{21}$$

where $u_{m_{\mathrm{PAH_{i,filt}}}}$ is the uncertainty of PAH mass detected by GC/MS from filter samples, $u_{\dot{V}_{\mathrm{filt}}}$ is the uncertainty of the volumetric flow through the filter samples, and $u_{\gamma_{\mathrm{filt}}}$ is the uncertainty of the surface area correction ratio.

Appendix E.1. Mass of detected PAH

The uncertainty of PAH mass detected by TD-GC/MS of a given species, i, regardless of TD tube or filter analyses, m_{PAH_i}, was estimated by combining type A and B evaluation of

uncertainty [34]. The type A evaluation of uncertainty is the standard deviation ($s_{m_{PAH_i}}$) in the measurements made during replicate GC/MS runs, and the type B evaluation of uncertainty is the reported bias in the instrumentation and calibration bias ($u_{m_{PAH_i,bias}}$).

$$u_{m_{\mathrm{PAH_i}}} = \sqrt{s^2_{m_{PAH_i}} + u^2_{m_{PAH_i,bias}}} \tag{22}$$

Appendix E.2. Volumetric sampling

Type B evaluation of uncertainty dominates for the uncertainty of the volumetric TD tube sampling flow rate, which is also at 5 % of the reading. Therefore, the uncertainty of the volumetric flow rate through the TD tube is approximately the uncertainty of the pump.

$$u_{\dot{V}_{\mathrm{TD}}} \approx u_{\mathrm{inst}} \tag{23}$$

The uncertainty of the volumetric filter sampling flow rate is presented in D.3. The uncertainty of the surface area correction ratio, $u_{\gamma_{\mathrm{filt}}}$, is based on the uncertainties of the diameter of where the soot samples are collected on the filter, d_{filt}, and the diameter of the individual punch outs, d_{po} (Eq. 7).

$$u_{\gamma_{\mathrm{filt}}} = \sqrt{\left(\frac{\partial \gamma_{\mathrm{filt}}}{\partial d_{\mathrm{filt}}} u_{d_{\mathrm{filt}}}\right)^2 + \left(\frac{\partial \gamma_{\mathrm{filt}}}{\partial d_{\mathrm{po}}} u_{d_{\mathrm{po}}}\right)^2} \tag{24}$$

for both diameter measurements, type B evaluation of uncertainty for the caliper used to measure the diameter is < 1 % of the reading. Therefore, the uncertainty of the diameters is approximately the uncertainty from type A which is the measurement standard deviation.

$$u_{d_{\mathrm{filt}}} \approx s_{d_{\mathrm{filt}}} \tag{25}$$

$$u_{d_{\mathrm{po}}} \approx s_{d_{\mathrm{po}}} \tag{26}$$

Appendix F. Uncertainty of the Total PAH Yield

The uncertainty of the total PAH yield is estimated using propagation of uncertainty on Eq. 9.

$$u_{y_{\mathrm{PAH_{tot}}}} = \sqrt{\left(\frac{\partial y_{\mathrm{PAH_{tot}}}}{\partial C_{\mathrm{PAH_{tot}}}} u_{C_{\mathrm{PAH_{tot}}}}\right)^2 + \left(\frac{\partial y_{\mathrm{PAH_{tot}}}}{\partial m_f} u_{m_f}\right)^2 + \left(\frac{\partial y_{\mathrm{PAH_{tot}}}}{\partial \dot{V}_a} u_{\dot{V}_a}\right)^2} \tag{27}$$

where $u_{C_{\mathrm{PAH_{tot}}}}$ is from E, u_{m_f} is from D.2, and $u_{\dot{V}_a}$ is from D.4.